Towards a Unified Evaluation of Explanation Methods without Ground Truth

Hao Zhang, Jiayi Chen, Haotian Xue, Quanshi Zhang[*]
Shanghai Jiao Tong University

Abstract

This paper proposes a set of criteria to evaluate the objectiveness of explanation methods of neural networks, which is crucial for the development of explainable AI, but it also presents significant challenges. The core challenge is that people usually cannot obtain ground-truth explanations of the neural network. To this end, we design four metrics to evaluate explanation results without ground-truth explanations. Our metrics can be broadly applied to nine benchmark methods of interpreting neural networks, which provides new insights of explanation methods.

1 Introduction

Nowadays, many methods are proposed to explain the feature representations of a deep neural network (DNN) in a post-hoc manner. In this research, we limit our attention to existing methods of estimating the *importance/attribution/saliency* of input pixels or intermediate-layer neural units *w.r.t.* the network output (Shrikumar et al., 2016; Lundberg & Lee, 2017; Ribeiro et al., 2016; Binder et al., 2016), which present the mainstream of explaining neural networks. To avoid ambiguity, the estimated importance/saliency/attribution maps are all termed "attribution maps" in this paper.

However, some methods usually pursue attribution maps which look reasonable from the perspective of human users, instead of objectively reflecting the information processing in the DNN. A trustworthy evaluation of the objectiveness of attribution maps is crucial for the development of deep learning and proposes significant challenges to state-of-the-art algorithms.

Existing metrics (Yang & Kim, 2019; Arras et al., 2019) of evaluating explanation methods have certain shortcomings.

Issue 1, evaluation of the accuracy of a DNN $\neq$ evaluation of the objectiveness of attribution maps: *Some methods only evaluate whether the visualized attribution map looks reasonable to human users, instead of examining whether an attribution map objectively reflects the truth of a DNN.* (Cui et al., 2019; Yang et al., 2019) used human cognition to evaluate the explanation result. (Yang & Kim, 2019; Kim et al., 2017; Camburu et al., 2019) aimed to construct a specific dataset with ground-truth explanations for evaluation. For example, they added an irrelevant object into the image. Pixels from the irrelevant object are expected to be assigned with zero attributions.

However, strictly speaking, it is impossible to religiously annotate ground-truth explanations for a DNN. Currently, the ground-truth explanation is constructed under the assumption that a DNN cannot learn irrelevant objects for classification. Its purpose was to evaluate attribution maps of the DNN, instead of examining whether an explanation method mistakenly generates seemingly correct attribution maps which do not reflect the truth of an incorrectly learned DNN.

Issue 2, broad applicability: We aim to design an evaluation metric that can be broadly applied to various tasks. In aforementioned methods (Yang & Kim, 2019; Kim et al., 2017; Camburu et al., 2019), the requirement for constructing a new testing dataset limits the applicability of the evaluation.

Issue 3, quantification of the objectiveness: Some methods quantitatively evaluate the accuracy and robustness of attribution maps. However, there is no strict mechanism to ensure the objectiveness

---

Table 1: Review of explanation methods

Method	What to explain	Qualitative evaluation of limitations in application
CAM (Zhou et al., 2016)	Attribution distribution at intermediate layer	1. Requirement for global average pooling. 2. Usually explain features at high layers
Grad_CAM (Selvaraju et al., 2017)	Attribution distribution at intermediate layer	Usually explain features at high layers
Grad (Simonyan et al., 2013)	Pixel-wise attribution	–
GI (Shrikumar et al., 2016)	Pixel-wise attribution	–
GB (Springenberg et al., 2014)	Pixel-wise attribution	Requirement for using ReLU as non-linear layers
Shapley Value (Shapley, 1953)	Pixel-wise attribution	NP-complete problem
DeepSHAP (Lundberg & Lee, 2017)	Pixel-wise attribution	Similar to LRP, DeepLIFT (Shrikumar et al., 2016) with a designed backward rule
LIME (Ribeiro et al., 2016)	Pixel-wise attribution	Attribution maps at the super-pixel level, rather than at the pixel level
LRP (Binder et al., 2016)	Pixel-wise attribution	Relevance propagation rules of every layer should be defined
Pert (Fong & Vedaldi, 2017)	Pixel-wise attribution	-

of each numerical value in the attribution map. *I.e.*, if the attribution value of a pixel is twice of that of another pixel, then the first pixel is supposed to contribute twice numerical values to the prediction *w.r.t.* the second pixel.

Except for the objectiveness, previous studies also conducted the evaluation from other perspectives. (Arras et al., 2019; Vu et al., 2019) evaluated attribution maps from the perspective of adversarial attacks by adding random noise. (Adebayo et al., 2018; Ghorbani et al., 2019; Alvarez-Melis & Jaakkola, 2018) proposed methods to evaluate the robustness of explanation methods *w.r.t.* the perturbation. (Adebayo et al., 2018) randomized the layer of DNN from the top to the bottom and visualized the change of attribution maps.

Considering the above three issues, in this study, we aim to fairly evaluate attribution maps generated by explanation methods without ground truth. The evaluation of attribution maps needs to be conducted from the following four perspectives, which are supplementary to each other, *i.e.*, objectiveness, completeness, robustness, and commonness. First, many explanation methods usually trade off between objectiveness and completeness, *i.e.*, choosing either to objectively report accurate attributions of salient (easy) regions, or to pay more attention to non-salient (difficult) regions for more complete explanation. On the other hand, we also analyze the robustness and commonness of explanations. Common explanations shared by different explanation methods are usually robust in real applications, although common explanations do not always objectively reflect the truth of a DNN. Note that in most applications, people cannot faithfully obtain ground-truth attribution maps. Therefore,the objectiveness, completeness, robustness, and commonness of explanation methods need to be evaluated without ground-truth, which is the distinct contribution compared to previous studies.

1. Objectiveness, bias of the attribution map at the pixel level: In order to evaluate the bias of the attribution map, we first need to propose a standard metric to evaluate the accuracy of explanation methods. The Shapley value is the unique solution to model the attribution value of each pixel that satisfies desirable properties including efficiency, symmetry and monotonicity (Lundberg & Lee, 2017). However, the computation of the Shapley value is an NP-complete problem, and previous studies (Lundberg & Lee, 2017) showed that the accurate estimation of the Shapley value is still a significant challenge. To this end, we extend the theory of Shapley sampling (Castro et al., 2009) and design a new evaluation metric, which achieves high accuracy without significantly boosting the computational cost.

We use the new evaluation metric to quantify the bias of the attribution map. Note that this evaluation has no partiality to the Shapley-value-based explanation methods. For example, experimental results showed that LRP (Binder et al., 2016) exhibited significantly lower bias than DeepSHAP (Lundberg & Lee, 2017).

2. Completeness, quantification of unexplainable feature components: Given an input image and its attribution map, we revise the input image to generate a new image in which we mask

unimportant regions. We then compare the intermediate-layer feature of the original image with that of the generated image, so as to disentangle feature components that can and cannot be explained by the attribution map.

3. Robustness, robustness of the explanation: Robustness of the explanation means whether the attribution map is robust to spatial masking of the input image. When we randomly mask a certain region of the input image, we admit that spatial masking destroys global contexts and affects pixel-wise attribution value to some extent. The quantification of the robustness of the explanation is an important perspective of evaluating an explanation method.

4. Commonness, mutual verification: The mutual verification means whether different explanation methods can verify each other. Methods generating similar attribution maps are usually believed more reliable.

In this paper, we used our metrics to evaluate nine widely used explanation methods listed in Table 1. We conducted experiments using the LeNet, VGG and ResNet on different benchmark datasets including the CIFAR-10 (Krizhevsky & Hinton, 2009) dataset and the Pascal VOC 2012 (Everingham et al., 2010) dataset. Our experimental results proved the effectiveness of the proposed evaluation methods and provided an insightful understanding of various explanation methods.

The contribution of our work can be concluded as follows.
- In this study, we invent a set of standard metrics to evaluate the objectiveness and the robustness of the attribution map without knowing ground-truth explanations.
- The metric of evaluating the pixel-wise bias of the attribution map can be estimated with a relatively low computational cost, which avoids falling into the computational bottleneck of estimating accurate pixel-wise attributions.
- Since our metrics do not need any annotations of ground-truth explanations, our metrics can be applied to different neural networks trained on different datasets.

2 RELATED WORK

Explainable AI is an emerging direction in artificial intelligence, and different explanation methods have been proposed.

Firstly, the visualization of feature representations inside a DNN is the most direct way of opening the black-box of the DNN. Related techniques include gradient-based visualization (Zeiler & Fergus, 2014; Mahendran & Vedaldi, 2015; Yosinski et al., 2015) and up-convolutional nets (Dosovitskiy & Brox, 2016). Secondly, other studies diagnose feature representations inside a DNN. (Kindermans et al., 2018) extracted rough pixel-wise correlations between network inputs and outputs, *i.e.*, estimating image regions with large influence on the network output. Network-attack methods (Koh & Liang, 2017; Szegedy et al., 2014) computed adversarial samples to diagnose a CNN. Bau *et al.* (Bau et al., 2017) defined six types of semantics for CNN filters, *i.e.* objects, parts, scenes, textures, materials, and colors. Fong and Vedaldi (Fong & Vedaldi, 2018) analyzed how multiple filters jointly represented a certain visual concept. Thirdly, a recent new trend is to learn interpretable features in DNNs (Hu et al., 2016; Stone et al., 2017; Liao et al., 2016). Capsule nets (Sabour et al., 2017) and interpretable RCNN (Wu et al., 2017) learned interpretable features in intermediate layers. InfoGAN (Chen et al., 2016) and β-VAE (Higgins et al., 2017) learned well-disentangled codes for generative neural networks.

However, to simplify the story, in this paper, we briefly review the Shapley value and limit our discussions to existing methods of evaluating methods of extracting attribution/importance/saliency maps.

The Shapley value: The Shapley value (Shapley, 1953) was proposed to compute the attribution distribution over all players in a particular cooperative game. However, it is an NP-complete problem to compute the accurate Shapley value. The Shapley value approximated by sampling strategy could be very inaccurate due to the high variance. We extend the theory of the Shapley value to obtain an evaluation metric with a high accuracy but a low computational cost.

Qualitative evaluation: Some studies used a qualitative criterion for evaluation. (Cui et al., 2019) qualitatively defined basic concepts in the evaluation of explanation results, including the complexity of the explanation, the correlation, and the completeness. (Yang et al., 2019) qualitatively evaluated

explanation methods according to their generalizability, fidelity and persuasibility. In contrast, this paper aims to evaluate the methods quantitatively, which makes our metrics more objective and reliable.

Accuracy evaluation: To evaluate the accuracy of attribution maps, (Arras et al., 2019; Vu et al., 2019) used the noise/occlusion to perturb the original image according to the attribution value. However, there was no mechanism to ensure the prediction result objectively reflected the truth of a DNN. (Yang & Kim, 2019; Kim et al., 2017) built a dataset to help them generate ground-truth explanations. Essentially, these methods tried to evaluate the correctness of attributions. However, a rigorous study should not assume that the DNN can make inference in the same way as people. (Oramas et al., 2019) proposed four metrics to evaluate the explanation from four different perspectives, which can provide a comprehensive understanding towards explanation methods. However, (Oramas et al., 2019) also used synthetic datasets and prediction results for evaluation. As a result, this paper proposes to evaluate the objectiveness of explanation results without annotations of ground-truth explanations.

Stability evaluation: (Adebayo et al., 2018; Ghorbani et al., 2019; Alvarez-Melis & Jaakkola, 2018) mainly paid attention to the attribution map change when the model input was perturbed. (Adebayo et al., 2018) visualized the change in the attribution map when the weights of the model were destroyed from the top to the bottom. (Ghorbani et al., 2019; Alvarez-Melis & Jaakkola, 2018) used the adversarial image to alter the attribution map. In comparison, we propose a metric to evaluate the robustness to spatial masking.

3 ALGORITHM

3.1 PRELIMINARIES: THE SHAPLEY VALUE

The Shapley value measures the instancewise feature importance ranking problem. Let Ω be the set of all pixels of an image I. I_P denotes an image that replaces all pixels in set $\Omega \setminus P$ with average pixel value over images. $F(I_P)$ denotes the scalar output of a DNN based on a subset of pixels $P \subset \Omega$. To compute the Shapley value of the i-th feature, (Shapley, 1953) considered all subsets of Ω not containing the i-th feature and defined the Shapley value A_i^* as follows:

$$A_i^* = \sum_{P \subset \Omega \setminus \{i\}} \frac{|P|!(|\Omega| - |P| - 1)!}{|P|!} \left[F(I_{P \cup \{i\}}) - F(I_P) \right] \tag{1}$$

It is the unique solution that satisfies several desirable properties to assign attribution value to each feature dimension in the input, which have been well introduced in (Chen et al., 2018). For convenience of the reader, we also summarize such properties in (Chen et al., 2018) in the supplementary material.

3.2 EVALUATING THE BIAS OF THE ATTRIBUTION MAP AT THE PIXEL LEVEL

In this section, we design a metric to accurately evaluate the objectiveness of the attribution map. Given an image $I \in \mathbf{I}$, let us consider the DNN F with a single scalar output $y = F(I)$. For DNNs with multiple outputs, existing methods usually explain each individual output dimension independently. Let $\{a_i\}$ denote the pixel-wise attribution map estimated by a specific explanation method. We aim to evaluate the bias of $\{a_i\}$. People usually formulate the network output as the sum of pixel-wise attribution value, *i.e.* the output y can be decomposed as follows.

$$y = b + \sum_{i \in \Omega} A_i, \qquad \text{s.t.} \quad A_i = \lambda a_i \tag{2}$$

b denotes the bias; i denotes the index of each pixel in the input image; Ω denotes the set of all pixels in the image. Aforementioned $\{A_i^*\}$ can be considered as the ground-truth of $\{A_i\}$ (Lundberg & Lee, 2017). Since many explanation methods (Selvaraju et al., 2017; Simonyan et al., 2013) mainly compute relative values of attributions $\{a_i\}$, instead of a strict attribution map $\{A_i\}$. We use λ to bridge $\{A_i\}$ and $\{a_i\}$. λ is a constant for normalization, which can be eliminated during the implementation of the evaluation.

The estimated attribution of each pixel can be assumed to follow a Gaussian distribution $A_i \sim \mathcal{N}(\mu_i, \sigma_i^2)$ (Castro et al., 2009). Attribution distributions of different pixels can be further assumed
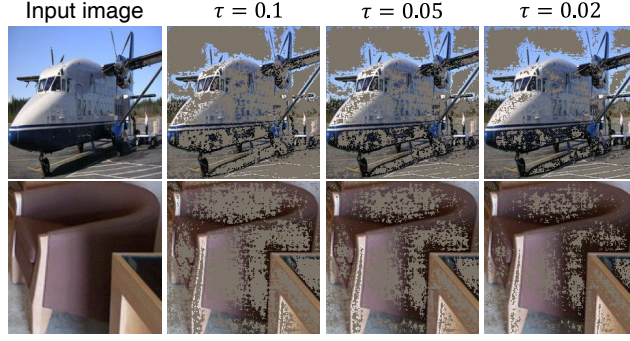
Figure 1: Masked image regions with different value of τ $(0 < \tau < 1)$. We need to set a small value of τ to make sure that unmasked image regions contain most attributions. When we set τ to 0.02, 0.05 and 0.1, the small difference of masked images doesn't significantly affect conclusion of the evaluation. Thus, we set $\tau = 0.05$ in this paper.

to share a unified variance, *i.e.* $\sigma_1^2 \approx \sigma_2^2 \approx ... \approx \sigma_n^2$. The evaluation of the attribution distribution $\{a_i\}$ has two aspects, *i.e.*

1. the sampling of pixels whose attributions are more likely to have large deviations;
2. the evaluation of the bias of the sampled attributions.

First, for the sampling of attributions of interest, we sample the set of pixels S with top-ranked high (or low) attributions. Attribution values of pixels in S are sampled as those with the highest (or the lowest) values, and these pixels are supposed to be more likely to be significantly biased towards high (or low) attribution values. Meanwhile, from another perspective, the distribution of the sampled attribution values is close to the Gumbel distribution.

Second, although the Shapley value can be considered as a standard formulation of the pixel-wise attribution, it usually cannot be accurately computed because of its high computational cost. In order to accurately evaluate the sampled attribution values without significantly increasing the computational cost, we applied the Shapley value approximated by the sampling method. Just like the target attribution distribution A_i, the approximated Shapley value A_i^{shap} is assumed to follow a normal distribution $\mathcal{N}(A_i^*, (\sigma^{shap})^2)$. A_i^{shap} is an unbiased approximation of the true Shapley value A_i^*, Thus, the average value over different pixels in S satisfies $\frac{\sum_{i \in S} A_i^{shap}}{|S|} \sim \mathcal{N}(\frac{\sum_{i \in S} A_i^*}{|S|}, \frac{(\sigma^{shap})^2}{|S|})$.

We can prove that the measurement of the average attribution among all sampled pixels $\frac{\sum_{i \in S} A_i^{shap}}{|S|}$ is of much higher accuracy than the raw Shapley value with the same computational cost. The difference between the highest (or lowest) values and its true values $\left| \frac{\sum_{i \in S} A_i^{shap}}{|S| \|A^{shap}\|} - \frac{\sum_{i \in S} A_i}{|S| \|A\|} \right|$ can reflect the system bias, as follows.

$$
\begin{aligned}
M_{\text{pixel}} &= \mathbb{E}_I \left[\left| \frac{\sum_{i \in S} A_i^{shap}}{|S| \|A^{shap}\|} - \frac{\sum_{i \in S} A_i}{|S| \|A\|} \right| \right] \\
&= \mathbb{E}_I \left[\frac{1}{|S|} \left| \frac{\sum_{i \in S} A_i^{shap}}{\|A^{shap}\|} - \frac{\sum_{i \in S} a_i}{\|a\|} \right| \right] \\
\text{s.t.} \quad &\forall i \in S, j \in \Omega \setminus S, a_i \geq a_j \\
\text{or} \quad &\forall i \in S, j \in \Omega \setminus S, a_i \leq a_j
\end{aligned}
\tag{3}
$$

where Ω is the set of all pixels in an image. $\|A^{shap}\|$ and $\|a\|$ are used for normalization. A small value of M_{pixel} indicates the low bias of the attribution map.

Analysis of the high computational efficiency: Suppose that the computational complexity of processing one sample is $\mathcal{O}(N)$, then the computational complexity of sampling m times is $\mathcal{O}(mN)$. If the raw Shapley value needs to obtain the same accuracy, it needs significantly more samples, and the computational complexity is $\mathcal{O}(|S|mN)$. Please see the supplementary material for further discussions about the computational cost.
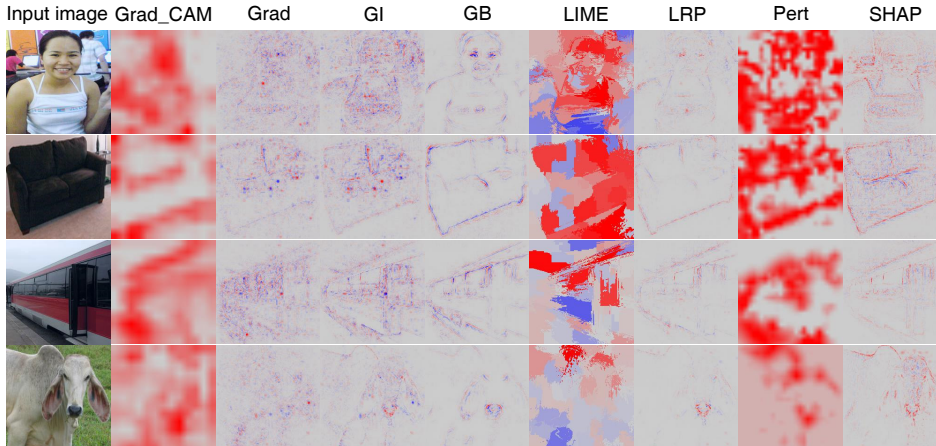
Figure 2: Examples of attribution maps of different methods. The supplementary material provides more attribution maps.

In addition, the proposed metric can also be used to evaluate the attribution of neural activations in the intermediate layer, such as those generated by Grad-CAM. In this case, we can regard the target intermediate-layer feature as the input image to compute attributions, so as to implement the evaluation. For each image, we need to sample multiple times to increase the accuracy. We compute the average performance over different images for evaluation. We need to sample multiple times with different images to increase the accuracy of the evaluation. Note that although the metric is designed based on the Shapley value, experimental results showed that LRP outperforms DeepSHAP.

3.3 QUANTIFICATION OF UNEXPLAINABLE FEATURE COMPONENTS

We propose another metric to quantify unexplainable feature components. Given an image I and its attribution map $\{a_i\}$, we generate a new image, which reflects the reasoning of the attribution map. In this way, we can consider the feature of the newly generated image $\widetilde{f}_I$ as feature components that can be explained. Let f_I denote the feature of the original image I. Then, $f_I - \widetilde{f}_I$ corresponds to the unexplainable feature components.

To generate the new image, we mask specific pixels in the original image I, which have the lowest attributions. We select and mask a set of pixels S with the lowest absolute attributions, and the number of the selected points is determined subjects to $\sum_{i \in S} |a_i| = \tau \sum_{i \in \Omega} |a_i|$ to generate the new image $\widetilde{I}$.

Note that τ is a small positive scalar to control the size of mask. In this study, we choose the value of τ as 0.05. As shown in the Figure 1, we set $\tau = 0.05$, *i.e.*, we mask pixels with lowest attributions. The masked pixels only make 5% attributions in total. In real application, the conclusion is not sensitive to the value of τ. Promising evaluation results obtained with $\tau = 0.05$ is similar to those obtained with $\tau = 0.1$. (Please see the supplementary material for results with $\tau = 0.1$.) The metric is formulated as

$$M_{\text{feature}} = \alpha \mathbb{E}_I \left[\| \widetilde{f}_I - f_I \| \right] \tag{4}$$

where $\alpha = \frac{1}{\mathbb{E}_{I'}[\| f_{I'} - \mathbb{E}_{I''}[f_{I''}] \|]}$ is used for normalization. A small value of M_{feature} indicates most feature components in f are explainable.

3.4 EVALUATING THE ROBUSTNESS OF EXPLANATION

This metric is used to measure the robustness of explanation methods to the spatial masking. We believe that the method, which is robust to spatial masking, can be considered more convincing. The robustness is an important perspective of evaluating explanation methods.

Given an input image $I \in \mathbf{I}$ and its attribution map $\{a_i\}$ *w.r.t* a DNN, we use a mask M to cover specific parts of the image to get a masked image $\hat{I}$. For each input image I, we can generate four
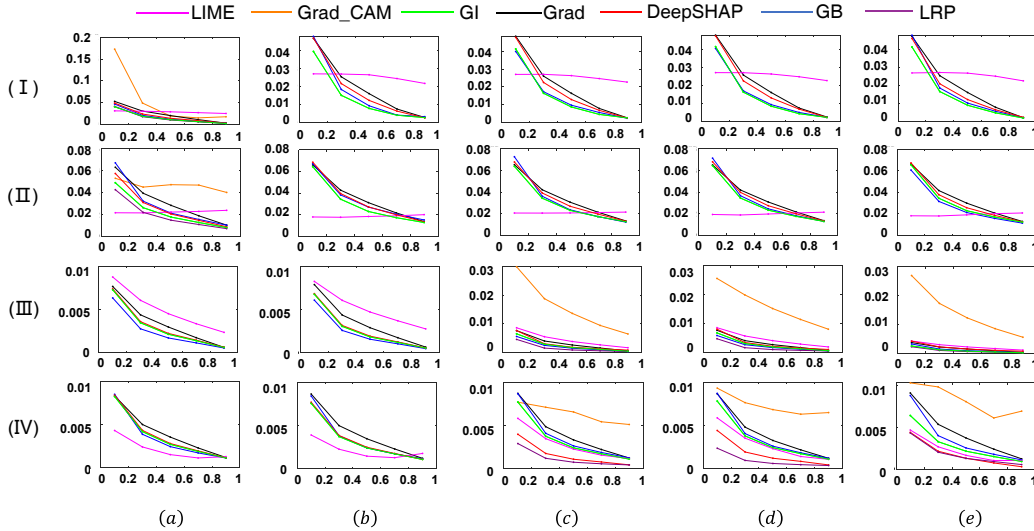
Figure 3: Results of the bias of the attribution map at the pixel level. Row (I) and row (II) used trained LeNet, ResNet20, ResNet32, ResNet44, ResNet56 on the CIFAR-10 dataset from left to right; row (III) and row (IV) used trained ResNet50, ResNet101, VGG16, VGG19, AlexNet on the Pascal VOC 2012 dataset from left to right. Row (I) and row (III) sampled pixels with the highest attribution values; row (II) and row (IV) sampled the pixels with the lowest attribution values. Explicit numbers in these curves are listed in the supplementary material.

masked images by masking the right, left, top, and bottom half of the image, respectively. For each masked image $\hat{I}$, the explanation method estimates the attribution $\hat{a}_i$ for each pixel. Note that for the masked image, we still compute attributions with respect to target classification result for fair comparisons. We compare pixel-level attributions of the unmask pixels between original images and masked images, as follows.

$$M_{\text{non-robust}} = \mathbb{E}_I \left[\frac{1}{\|a\|} \sqrt{\sum_{i \in I \setminus I_{mask}} (a_i - \hat{a}_i)^2} \right] \tag{5}$$

We used $\|a\|$ for normalization, and a large value of $M_{\text{non-robust}}$ indicates a high non-robustness.

3.5 EVALUATING THE MUTUAL VERIFICATION

This metric aims to quantitatively measure the mutual verification between different explanation methods. Adebayo *et al.* (Adebayo et al., 2018) showed that some methods generated similar explanations, but they were all unreliable and biased. However, such a metric still provided some new insights on the relationship between different explanation methods. Given a DNN F and an image $I \in \mathbf{I}$, two different explanation methods α and β produce attribution maps a_α and a_β, respectively. We measure their difference as follows.

$$M_{\text{mutual}} = \mathbb{E}_I \left[\| \frac{a_\alpha}{\|a_\alpha\|} - \frac{a_\beta}{\|a_\beta\|} \| \right] \tag{6}$$

Attribution maps from different explanation methods are normalized by their L2-norm. A lower value of M_{mutual} indicates a more convincing mutual verification between explanation methods α and β.

3.6 DISCUSSION ABOUT LIMITATIONS

Table 2 shows the limitation and applicability of these metrics. Note that different applications may have their own evaluation metrics. Nevertheless, in this paper, we focus on some common desir-

Table 2: Limitations of different evaluation metrics.

Metrics	Limitation & Applications
Bias of the attribution map	The method must calculate an attribution map with both positive and negative values.
Quantification of unexplainable feature components	The attribution map must be computed for pixels in the input image instead for units in the intermediate-layer feature.
Robustness of explanation method	We only evaluate the robustness towards spatial masking. There can be other kinds of robustness.
Mutual verification	The compared attribution maps must be calculated for the same item (*e.g.* input image or intermediate feature).

Table 3: Quantification of unexplainable feature components with $\tau = 0.05$. LIME usually outperformed other explanation methods.

Method	Grad	GI	GB	DeepSHAP	LIME	LRP	Pert
CIFAR10-LeNet	0.82971	0.98173	0.81278	0.98706	**0.54371**	0.97856	0.58968
CIFAR10-ResNet20	1.11988	1.21033	1.09124	1.20117	**0.93836**	-	1.05067
CIFAR10-ResNet32	1.16659	1.22853	1.12193	1.20667	**0.91767**	-	1.07155
CIFAR10-ResNet44	1.13872	1.19983	1.03684	1.1786	**0.89585**	-	1.01908
CIFAR10-ResNet56	1.12963	1.18625	1.05485	1.17067	**0.89013**	-	1.02354
VOC2012-AlexNet	0.91919	0.99364	0.97473	0.98271	**0.89007**	1.02604	0.9409
VOC2012-VGG16	1.11413	1.13402	1.16247	1.23222	**0.98048**	1.25679	1.01887
VOC2012-VGG19	1.00716	1.06308	1.04998	1.11102	**0.95401**	1.17729	1.02434
VOC2012-ResNet50	1.17766	1.19739	1.18706	1.19072	**1.15894**	-	1.20921
VOC2012-ResNet101	**0.99979**	1.01592	1.04046	1.0095	1.01902	-	1.18937

able properties that need to be shared by evaluation metrics, *i.e.* the objectiveness, completeness, robustness, and commonness. They provide new insights on explanation methods.

4 EXPERIMENT

To evaluate explanation methods, we conducted experiments on the CIFAR-10 (Krizhevsky & Hinton, 2009) dataset and the Pascal VOC 2012 (Everingham et al., 2010) dataset. The Pascal VOC 2012 dataset is mainly used for object detection. Just like in (Zhang et al., 2018), we cropped objects using their bounding boxes. We used the cropped objects as inputs to train DNNs for multi-category classification. We trained and explained LeNet (LeCun et al., 1998), ResNet-20/32/44/56 (He et al., 2016) using the CIFAR-10 dataset. AlexNet (Krizhevsky et al., 2012), VGG-16/19 (Simonyan & Zisserman, 2015), ResNet-50/101 (He et al., 2016) were trained using the Pascal VOC 2012 dataset.

4.1 BASELINE

In our experiments, we mainly evaluated the following explanation methods. Figure 2 shows attribution maps yielded by these explanation methods.

Grad: Given an input, (Simonyan et al., 2013) quantified the attribution value with the gradient of the input. We termed this algorithm as Grad. For RGB images with multiple channels, Grad selected the maximum magnitude across all channels for each pixel.

GI: (Shrikumar et al., 2016) proposed a method, namely GI, which used the pixel-wise product of the input and its gradient as attribution value. Attribution values for RGB channels were summed to get the final attribution value.

GB: Guided Back-propagation, namely GB, corresponded to Grad where the back-propagation rule at ReLU units was redefined (Springenberg et al., 2014).

LRP: Layer-wise relevance propagation (LRP) (Binder et al., 2016) redefined back-propagation rules for each layer to decompose the output of a DNN over the input. We used LRP-ϵ and set the parameter $\epsilon = 1$ in experiments.

DeepSHAP: DeepSHAP adapted DeepLIFT (Shrikumar et al., 2016) to approximate pixel-wise Shapley values for the input image (Lundberg & Lee, 2017). We applied the code released by (Lundberg & Lee, 2017).

LIME: LIME (Ribeiro et al., 2016) trained an interpretable model to compute the attribute value for each super-pixel. We used the code released by (Ribeiro et al., 2016).

Table 4: Non-robustness of explanation methods with different datasets/models. GB and Grad_CAM had the lowest non-robustness. For more results, the supplementary material shows examples of attribution maps of masked images.

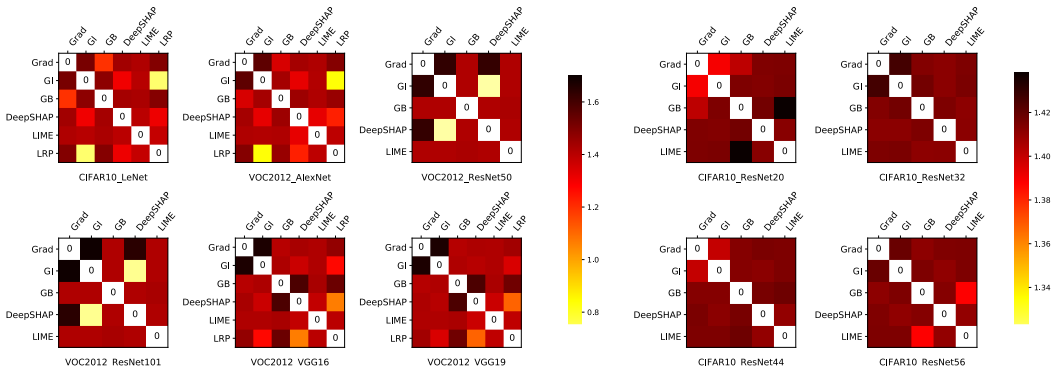| Method	Grad	GI	GB	LIME	LRP	Pert	CAM	Grad_CAM
CIFAR10-LeNet	0.503	0.608	0.473	6.799	1.139	**0.472**	-	1.302
CIFAR10-ResNet20	0.466	0.545	**0.299**	1.199	-	0.455	0.422	0.394
CIFAR10-ResNet32	0.661	0.733	**0.301**	1.626	-	0.458	0.399	0.400
CIFAR10-ResNet44	0.809	0.866	**0.269**	1.239	-	0.466	0.358	0.349
CIFAR10-ResNet56	0.752	0.794	**0.289**	3.023	-	0.447	0.376	0.372
VOC2012-AlexNet	0.439	0.519	**0.359**	1.698	0.654	0.678	-	0.442
VOC2012-VGG16	0.362	0.382	**0.239**	3.597	0.378	0.607	-	0.308
VOC2012-VGG19	0.384	0.398	**0.256**	2.074	0.393	0.653	-	0.303
VOC2012-ResNet50	0.548	0.605	**0.258**	1.538	-	0.518	0.290	0.308
VOC2012-ResNet101	0.460	0.493	**0.225**	1.408	-	0.525	0.248	0.296

Figure 4: Heat maps of mutual verification. A low value of M_{mutual} between two methods indicates a more convincing mutual verification between them, *e.g.* LRP and GI had convincing results of mutual verification. The supplementary material provides more numerical results.

Pert: (Fong & Vedaldi, 2017) explained a prediction by training a mask to perturb the input image. Mask values ranging between 0 and 1 indicated the saliency of each pixel. We termed this method Pert.

CAM: CAM computed attribution map over the feature from the last convolutional layer (Zhou et al., 2016). It required the special structure with a global average pooling layer and a fully connected layer at the end of the DNN.

Grad_CAM: Grad_CAM was similar to CAM (Selvaraju et al., 2017). Grad_CAM used gradients over the feature map, instead of the parameters of the fully connected layer.

4.2 IMPLEMENTATION DETAILS

Bias of the attribution map at the pixel level: To approximate the Shapley value for each image, we sampled 1000 times for each image in the CIFAR-10 dataset and sampled 100 times for each image in the Pascal VOC 2012 dataset. We sampled the top-10%, 30%, 50%, 70%, 90% pixels with the highest/lowest values.

Quantification of unexplainable feature components: Given an image, we masked the pixels with the lowest absolute attribution value. The number of the masked pixels was determined to ensure that the sum of masked absolute attribution value took 5% of the total absolute attribution value. On average, around 30% pixels were masked. The masked pixels were assigned with the average pixel value over images. We used features of the last convolutional layer to compute M_{feature}.

4.3 EXPERIMENT RESULT AND ANALYSIS

Bias of the attribution map at the pixel level: Figure 3 shows curves of evaluation results on different models learned using different datasets. According to these curves, GI and GB provided the least biased attribution maps for ResNet at the pixel level. For AlexNet, VGG-16/19 and LeNet, LRP outperformed other methods. Besides, we found that the performance of LIME was volatile, *i.e.* in some cases, LIME performed quite well, but in some other cases, LIME performed worst. This situation was obvious on the CIFAR-10 dataset. We believed that it was because LIME calculated attribution maps for super-pixels. The number of super-pixels in an image from CIFAR-10 dataset was limited. In this way, many pixels within a single super-pixel shared the same attribution value in results of LIME, which made it hard to sample these pixels with significantly biased attribution values.

Some methods could not be evaluated using the bias at the pixel level. For example, Pert computed an importance map without negative values instead of an attribution map for each image. The code of CAM (Zhou et al., 2016) projected attribution values to the range between 0 and 1. Grad_CAM and LRP were not used on residual networks. Because there was only one fully connected layer behind the last convolutional layer in residual networks, in this case, Grad_CAM could not reflect the information processing contained in the cascaded non-liner layers of the DNN. For LRP, the relevance propagation rules of some structures in ResNet were not defined to the best of our knowledge.

Quantification of unexplainable feature components: Table 3 compares the amount of unexplainable feature components between explanation methods. We found that LIME, GB and Pert explained more feature components than other methods. We noticed that the quantification of unexplainable feature components of most explanation methods were considerable larger than expected. It was because the attribution maps from some methods contained relatively larger noise. Thus, the masked pixels were almost uniformly distributed over images, which destroyed the context information and led to worse results.

We did not evaluate CAM and Grad_CAM, because they calculated attribution maps at the feature level, which were not comparable with attribution values at the pixel level.

Robustness of explanation: Table 4 shows the quantitative results of $M_{\text{non-robust}}$ on different models trained using different datasets. We found that GB and Grad_CAM exhibited a lower non-robustness to spatial masking. LIME segmented the input image into super pixels to calculate attributions, and the spatial masking could influence the segmentation result significantly. Thus, non-robustness of LIME was much higher than other explanation methods.

Mutual verification: Figure 4 visualizes the mutual verification M_{mutual} between different explanation methods, which indicates a high level mutual verification between LRP, GI and DeepSHAP. Note that we did not compare CAM and Grad_CAM with other methods. It was because they computed attribution maps on intermediate-layer features.

5 CONCLUSION

In this paper, we have proposed four metrics to evaluate explanation methods from four different perspectives. The proposed evaluation metrics are computed without requirements for ground-truth explanations. Our metrics can be applied to widely used explanation methods *w.r.t.* different DNNs learned using different datasets. These metrics evaluate the bias of the attribution map at the pixel level, quantify the unexplainable feature components, the robustness of the explanation and the mutual verification. In experiments, we used our metrics to evaluate nine widely used explanation methods. Experimental results showed that attribution maps from LRP, GI and GB exhibited lower bias at the pixel level. LIME and GB explained more feature components than other methods. Regarding the robustness, GB, CAM and Grad_CAM were more robust to spatial masking than other explanation methods. DeepSHAP, GI and LRP can better verified each other.

REFERENCES

Julius Adebayo, Justin Gilmer, Michael Muelly, Ian Goodfellow, Moritz Hardt, and Been Kim. Sanity checks for saliency maps. *In NIPS*, 2018.

David Alvarez-Melis and Tommi S. Jaakkola. Towards robust interpretability with self-explaining neural networks. *In arXiv:1806.07538*, 2018.

Leila Arras, Ahmed Osman, Klaus-Robert Müller, and Wojciech Samek. Evaluating recurrent neural network explanations. *In arXiv:1904.11829*, 2019.

David Bau, Bolei Zhou, Aditya Khosla, Aude Oliva, and Antonio Torralba. Network dissection: Quantifying interpretability of deep visual representations. *In CVPR*, 2017.

Alexander Binder, Grégoire Montavon, Sebastian Lapuschkin, Klaus-Robert Müller, and Wojciech Samek. Layer-wise relevance propagation for neural networks with local renormalization layers. *In International Conference on Artificial Neural Networks (ICANN)*, 2016.

Oana-Maria Camburu, Eleonora Giunchiglia, Jakob Foerster, Thomas Lukasiewicz, and Phil Blunsom. Can i trust the explainer? verifying post-hoc explanatory methods. *arXiv: 1910.02065*, 2019.

Javier Castro, Daniel Gómez, and Juan Tejada. Polynomial calculation of the shapley value based on sampling. *In Computers & Operations Research*, 36(5):1726–1730, 2009.

Jianbo Chen, Le Song, Martin J. Wainwright, and Michael I. Jordan. L-shapley and c-shapley: Efficient model interpretation for structured data. *In arXiv:1808.02610*, 2018.

Xi Chen, Yan Duan, Rein Houthooft, John Schulman, Ilya Sutskever, and Pieter Abbeel. Infogan: Interpretable representation learning by information maximizing generative adversarial nets. *In NIPS*, 2016.

Xiaocong Cui, Jung Min Lee, and J Hsieh. An integrative 3c evaluation framework for explainable artificial intelligence. *In The annual Americas Conference on Information Systems (AMCIS)*, 2019.

Alexey Dosovitskiy and Thomas Brox. Inverting visual representations with convolutional networks. *In CVPR*, 2016.

M. Everingham, L. Van Gool, C. K. I. Williams, J. Winn, and A. Zisserman. The pascal visual object classes (voc) challenge. *In International Journal of Computer Vision*, 88(2):303–338, June 2010.

Ruth Fong and Andrea Vedaldi. Net2vec: Quantifying and explaining how concepts are encoded by filters in deep neural networks. *In CVPR*, 2018.

Ruth C. Fong and Andrea Vedaldi. Interpretable explanations of black boxes by meaningful perturbation. *In arXiv:1704.03296v1*, 2017.

Amirata Ghorbani, Abubakar Abid, and James Zou. Interpretation of neural networks is fragile. *In AAAI*, 2019.

Kaiming He, Xiangyu Zhang, Shaoqing Ren, and Jian Sun. Deep residual learning for image recognition. *In CVPR*, 2016.

Irina Higgins, Loic Matthey, Arka Pal, Christopher Burgess, Xavier Glorot, Matthew Botvinick, Shakir Mohamed, and Alexander Lerchner. β-vae: learning basic visual concepts with a constrained variational framework. *In ICLR*, 2017.

Zhiting Hu, Xuezhe Ma, Zhengzhong Liu, Eduard Hovy, and Eric P. Xing. Harnessing deep neural networks with logic rules. *In arXiv:1603.06318v2*, 2016.

Been Kim, Martin Wattenberg, Justin Gilmer, Carrie Cai, James Wexler, Fernanda Viegas, and Rory Sayres. Interpretability beyond feature attribution: Quantitative testing with concept activation vectors (tcav). *In arXiv:1711.11279*, 2017.

Pieter-Jan Kindermans, Kristof T. Schütt, Maximilian Alber, Klaus-Robert Müller, Dumitru Erhan, Been Kim, and Sven Dähne. Learning how to explain neural networks: Patternnet and patternattribution. *In ICLR*, 2018.

PangWei Koh and Percy Liang. Understanding black-box predictions via influence functions. *In ICML*, 2017.

A. Krizhevsky and G. Hinton. Learning multiple layers of features from tiny images. *In Computer Science Department, University of Toronto, Tech. Rep*, 1, 2009.

Alex Krizhevsky, Ilya Sutskever, and Geoffrey E. Hinton. Imagenet classification with deep convolutional neural networks. *In NIPS*, 2012.

Yann LeCun, Lèon Bottou, Yoshua Bengio, and Patrick Haffner. Gradient-based learning applied to document recognition. *In Proceedings of the IEEE*, 1998.

Renjie Liao, Alex Schwing, Richard Zemel, and Raquel Urtasun. Learning deep parsimonious representations. *In NIPS*, 2016.

Scott M. Lundberg and Su-In Lee. A unified approach to interpreting model predictions. *In NIPS*, 2017.

Aravindh Mahendran and Andrea Vedaldi. Understanding deep image representations by inverting them. *In CVPR*, 2015.

Jose Oramas, Kaili Wang, and Tinne Tuytelaars. Visual explanation by interpretation: Improving visual feedback capabilities of deep neural networks. 2019.

Marco Tulio Ribeiro, Sameer Singh, and Carlos Guestrin. "why should i trust you?" explaining the predictions of any classifier. *In KDD*, 2016.

Sara Sabour, Nicholas Frosst, and Geoffrey E. Hinton. Dynamic routing between capsules. *In NIPS*, 2017.

Ramprasaath R. Selvaraju, Michael Cogswell, Abhishek Das, Ramakrishna Vedantam, Devi Parikh, and Dhruv Batra. Grad-cam: Visual explanations from deep networks via gradient-based localization. *In ICCV*, 2017.

Lloyd S Shapley. A value for n-person games. *In Contributions to the Theory of Games*, 2(28): 307–317, 1953.

Avanti Shrikumar, Peyton Greenside, Anna Shcherbina, and Anshul Kundaje. Not just a black box: Learning important features through propagating activation differences. *In arXiv:1605.01713*, 2016.

Karen Simonyan and Andrew Zisserman. Very deep convolutional networks for large-scale image recognition. *In ICLR*, 2015.

Karen Simonyan, Andrea Vedaldi, and Andrew Zisserman. Deep inside convolutional networks: Visualising image classification models and saliency maps. *In arXiv:1312.6034*, 2013.

Jost Tobias Springenberg, Alexey Dosovitskiy, Thomas Brox, and Martin Riedmiller. Striving for simplicity: The all convolutional net. *In arXiv:1412.6806*, 2014.

Austin Stone, Huayan Wang, Yi Liu, D. Scott Phoenix, and Dileep George. Teaching compositionality to cnns. *In CVPR*, 2017.

Christian Szegedy, Wojciech Zaremba, Ilya Sutskever, Joan Bruna, Dumitru Erhan, Ian Goodfellow, and Rob Fergus. Intriguing properties of neural networks. *In arXiv:1312.6199v4*, 2014.

Minh N Vu, Truc D Nguyen, NhatHai Phan, Ralucca Gera, and My T Thai. Evaluating explainers via perturbation. *In arXiv:1906.02032*, 2019.

Tianfu Wu, Xilai Li, Xi Song, Wei Sun, Liang Dong, and Bo Li. Interpretable r-cnn. *In arXiv:1711.05226*, 2017.

Fan Yang, Mengnan Du, and Xia Hu. Evaluating explanation without ground truth in interpretable machine learning. *In arxiv: 1907.06831*, 2019.

Mengjiao Yang and Been Kim. Bim: Towards quantitative evaluation of interpretability methods with ground truth. *In arXiv:1907.09701*, 2019.

Jason Yosinski, Jeff Clune, Anh Nguyen, Thomas Fuchs, and Hod Lipson. Understanding neural networks through deep visualization. *In ICML Deep Learning Workshop*, 2015.

Matthew D. Zeiler and Rob Fergus. Visualizing and understanding convolutional networks. *In ECCV*, 2014.

Quanshi Zhang, Ying Nian Wu, and Song-Chun Zhu. Interpretable convolutional neural networks. *In CVPR*, 2018.

Bolei Zhou, Aditya Khosla, Agata Lapedriza, Aude Oliva, and Antonio Torralba. Learning deep features for discriminative localization. *In CVPR*, 2016.

A   PROPERTIES OF THE SHAPLEY VALUE

Let I denote the input image; let Ω denote the set of all pixels in I. We can use $I_\emptyset$ to denote a baseline image, *i.e.* all pixels in $I_\emptyset$ equal to the average value over all images. For a subset $S \subset \Omega$, I_S denotes an image that satisfies

$$(I_S)_i = \begin{cases} (I)_i, & i \in S \\ (I_\emptyset)_i, & i \notin S \end{cases} \tag{7}$$

where i is the index of the pixel in I and I_Ω is the same image as I. Let F and G denote two models with scalar output. The Shapley value of the i-th pixel is represented by A_i^*, and they have the following properties Shapley (1953).

Efficiency: The sum of Shapley values $\sum_{i \in \Omega} A_i^*$ is equal to $F(I_\Omega) - F(I_\emptyset)$.

Symmetry: The features that are treated equally by the model are treated equally by the Shapley value. If $F(I_{S \cup \{i\}}) = F(I_{S \cup \{j\}})$ for all subsets S, then $A_i^* = A_j^*$.

Additivity: For any two models F and G, if they are combined into one model $F + G$, the Shapley value must be added pixel by pixel: $(A^*)_i^{F+G} = (A^*)_i^F + (A^*)_i^G$.

Monotonicity: For any two models F and G, if for all subsets S we have $F(I_{S \cup \{i\}}) - F(I_S) \geq G(I_{S \cup \{i\}}) - G(I_S)$ for all subsets S, then we have $(A^*)_i^F \geq (A^*)_i^G$.

B   ANALYSIS OF THE COMPUTATIONAL COST

In this section, we continue using the notation in Section 3.1 and Section 3.2. Suppose that we sample m times to approximate the Shapley value. The variance of A_i^{shap} is $\frac{\sigma^2}{m}$ where σ^2 satisfies Castro et al. (2009)

$$\sigma^2 = \sum_{P \subset \Omega \setminus \{i\}} \frac{|P|!(|\Omega| - |P| - 1)!}{|P|!} \left[F(I_{P \cup \{i\}}) - F(I_P) - A_i^* \right]^2 \tag{8}$$

So we have $(\sigma^{shap})^2 = \sigma^2/m$. For the set of sampled pixels S, the variance of their average Shapley value is $\frac{|S|(\sigma^{shap})^2}{|S|^2} = \frac{(\sigma^{shap})^2}{|S|} = \frac{\sigma^2}{m|S|}$. Apparently, if we want to get the same accuracy for a single pixel as the set of pixels, we need to sample $m|S|$ times, which needs much more computational cost than our metric, especially when the number of sampled pixels is large.

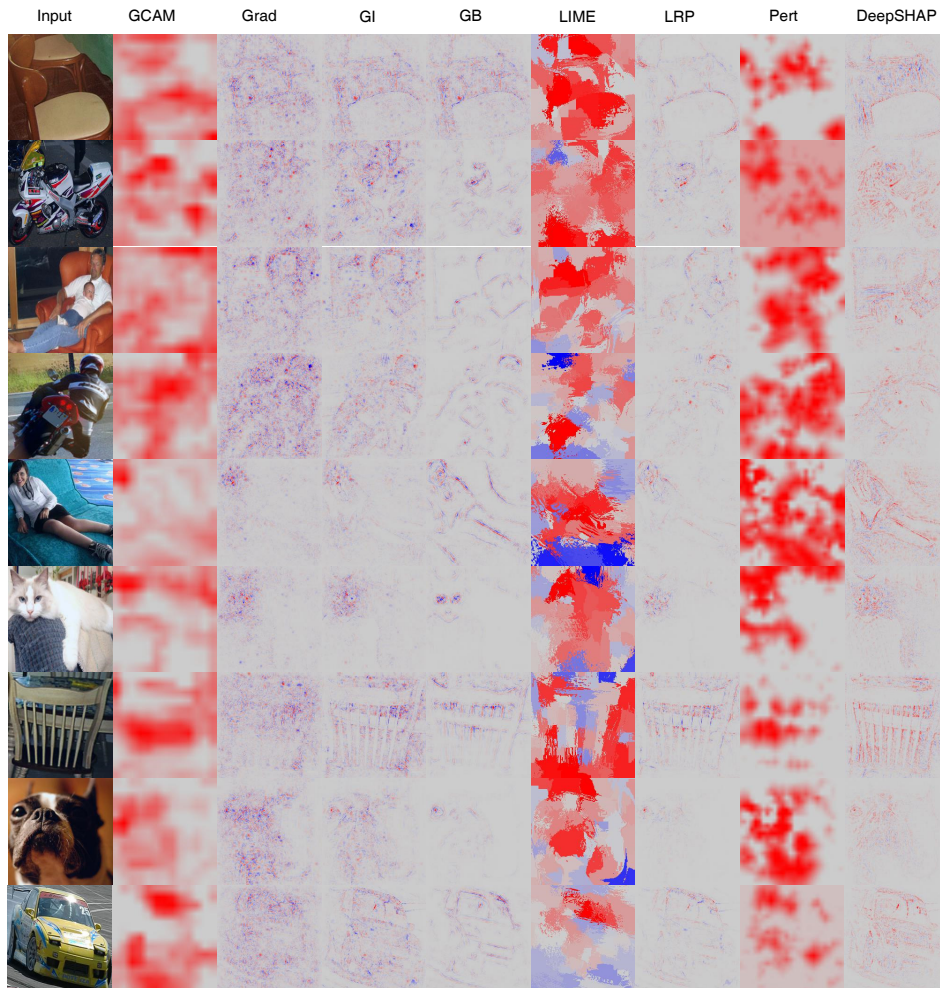# C   MORE EXAMPLES OF ATTRIBUTION MAPS

Figure 5: Examples of attribution maps.

D DETAILED RESULTS OF THE BIAS OF THE ATTRIBUTION MAP AT THE PIXEL LEVEL

Table 5: Bias of the attribution map at the pixel level on CIFAR-10-LeNet

Method	Grad_CAM	|Grad|	GI	GB	DeepSHAP	LIME	LRP
top-10%	0.17256	0.05302	0.04060	0.04701	0.04924	**0.03138**	0.04164
top-30%	0.04921	0.03090	0.01892	0.02109	0.02408	0.03051	**0.01798**
top-50%	0.01961	0.02057	0.01126	0.01225	0.01443	0.02919	**0.01041**
top-70%	0.01531	0.01137	0.00671	0.00746	0.00902	0.02727	**0.00634**
top-90%	0.01785	0.00314	**0.00240**	0.00300	0.00334	0.02537	0.00277
bottom-10%	0.05317	0.06326	0.04907	0.06730	0.05755	**0.02160**	0.04271
bottom-30%	0.04510	0.03948	0.02626	0.03224	0.03100	**0.02150**	0.02198
bottom-50%	0.04732	0.02840	0.01767	0.02126	0.02047	0.02222	**0.01481**
bottom-70%	0.04693	0.01886	0.01270	0.01551	0.01462	0.02286	**0.01086**
bottom-90%	0.04022	0.01026	0.00808	0.01025	0.00882	0.02385	**0.00708**

Table 6: Bias of the attribution map at the pixel level on CIFAR-10-ResNet20

Method	|Grad|	GI	GB	DeepSHAP	LIME
top-10%	0.04692	0.03962	0.04801	0.04702	**0.02716**
top-30%	0.02552	**0.01522**	0.01848	0.02175	0.02706
top-50%	0.01616	**0.00795**	0.00943	0.01241	0.02666
top-70%	0.00762	**0.00416**	0.00425	0.00643	0.02456
top-90%	0.00288	0.00283	0.00336	**0.00270**	0.02185
bottom-10%	0.06610	0.06449	0.06726	0.06866	**0.01790**
bottom-30%	0.04272	0.03437	0.03833	0.03962	**0.01765**
bottom-50%	0.03117	0.02296	0.02704	0.02722	**0.01836**
bottom-70%	0.02168	0.01726	0.02053	0.01992	**0.01897**
bottom-90%	0.01357	**0.01275**	0.01513	0.01346	0.02005

Table 7: Bias of the attribution map at the pixel level on CIFAR-10-ResNet32

Method	|Grad|	GI	GB	DeepSHAP	LIME
top-10%	0.04836	0.04126	0.03984	0.04773	**0.02699**
top-30%	0.02600	**0.01641**	0.01728	0.02247	0.02702
top-50%	0.01639	**0.00874**	0.00972	0.01289	0.02630
top-70%	0.00793	**0.00459**	0.00565	0.00683	0.02465
top-90%	0.00268	0.00264	**0.00242**	0.00260	0.02267
bottom-10%	0.06535	0.06389	0.07271	0.06787	**0.02059**
bottom-30%	0.04217	0.03433	0.03612	0.03917	**0.02053**
bottom-50%	0.03064	0.02304	0.02359	0.02686	**0.02065**
bottom-70%	0.02135	**0.01726**	0.01733	0.01963	0.02103
bottom-90%	0.01331	0.01254	**0.01214**	0.01307	0.02145

Table 8: Bias of the attribution map at the pixel level on CIFAR-10-ResNet44

Method	|Grad|	GI	GB	DeepSHAP	LIME
top-10%	0.04795	0.04155	0.04055	0.04751	**0.02712**
top-30%	0.02576	**0.01626**	0.01698	0.02254	0.02709
top-50%	0.01609	**0.00848**	0.00935	0.01307	0.02637
top-70%	0.00748	**0.00433**	0.00502	0.00686	0.02485
top-90%	0.00248	0.00228	0.00230	**0.00226**	0.02271
bottom-10%	0.06510	0.06452	0.07143	0.06802	**0.01924**
bottom-30%	0.04196	0.03449	0.03663	0.03977	**0.01879**
bottom-50%	0.03082	0.02323	0.02448	0.02736	**0.01967**
bottom-70%	0.02159	**0.01752**	0.01811	0.01989	0.02064
bottom-90%	0.01353	**0.01282**	0.01293	0.01323	0.02137

Table 9: Bias of the attribution map at the pixel level on CIFAR-10-ResNet56

Method	|Grad|	GI	GB	DeepSHAP	LIME
top-10%	0.04716	0.04129	0.04780	0.04601	**0.02690**
top-30%	0.02537	**0.01659**	0.01855	0.02089	0.02714
top-50%	0.01607	**0.00900**	0.01022	0.01215	0.02679
top-70%	0.00791	**0.00482**	0.00569	0.00652	0.02509
top-90%	0.00212	**0.00194**	0.00214	0.00234	0.02252
bottom-10%	0.06625	0.06551	0.06065	0.06727	**0.01828**
bottom-30%	0.04164	0.03449	0.03158	0.03779	**0.01812**
bottom-50%	0.03001	0.02299	0.02129	0.02574	**0.01911**
bottom-70%	0.02086	**0.01712**	0.01587	0.01868	0.02023
bottom-90%	0.01300	0.01237	**0.01146**	0.01267	0.02088

Table 10: Bias of the attribution map at the pixel level on VOC2012-ResNet50

Method	|Grad|	GI	GB	DeepSHAP	LIME
top-10%	0.00766	0.00728	**0.00633**	0.00738	0.00876
top-30%	0.00437	0.00345	**0.00276**	0.00359	0.00606
top-50%	0.00297	0.00213	**0.00170**	0.00223	0.00451
top-70%	0.00173	0.00138	**0.00113**	0.00144	0.00335
top-90%	0.00060	0.00060	**0.00053**	0.00062	0.00235
bottom-10%	0.00831	0.00824	0.00850	0.00839	**0.00430**
bottom-30%	0.00500	0.00417	0.00386	0.00432	**0.00240**
bottom-50%	0.00354	0.00269	0.00244	0.00280	**0.00151**
bottom-70%	0.00228	0.00189	0.00171	0.00194	**0.00113**
bottom-90%	0.00117	0.00112	**0.00111**	0.00114	0.00128

Table 11: Bias of the attribution map at the pixel level on VOC2012-ResNet101

Method	|Grad|	GI	GB	DeepSHAP	LIME
top-10%	0.00790	0.00678	**0.00610**	0.00685	0.00827
top-30%	0.00438	0.00307	**0.00260**	0.00318	0.00608
top-50%	0.00291	0.00185	**0.00158**	0.00194	0.00473
top-70%	0.00175	0.00121	**0.00104**	0.00127	0.00371
top-90%	0.00067	0.00055	**0.00049**	0.00056	0.00278
bottom-10%	0.00861	0.00754	0.00839	0.00767	**0.00387**
bottom-30%	0.00496	0.00369	0.00377	0.00381	**0.00222**
bottom-50%	0.00343	0.00237	0.00238	0.00245	**0.00142**
bottom-70%	0.00225	0.00169	0.00169	0.00173	**0.00124**
bottom-90%	0.00117	**0.00104**	0.00112	0.00105	0.00174

Table 12: Bias of the attribution map at the pixel level on VOC2012-AlexNet

Method	Grad_CAM	|Grad|	GI	GB	DeepSHAP	LIME	LRP
top-10%	0.05403	0.00744	0.00505	0.00646	0.00845	0.00854	**0.00453**
top-30%	0.03467	0.00434	0.00243	0.00296	0.00447	0.00598	**0.00197**
top-50%	0.02459	0.00298	0.00149	0.00182	0.00295	0.00443	**0.00119**
top-70%	0.01711	0.00176	0.00094	0.00120	0.00209	0.00329	**0.00080**
top-90%	0.01115	0.00060	**0.00035**	0.00058	0.00140	0.00222	0.00043
bottom-10%	0.01026	0.00906	0.00638	0.00876	0.00438	0.00466	**0.00430**
bottom-30%	0.00978	0.00534	0.00327	0.00400	0.00215	0.00267	**0.00202**
bottom-50%	0.00803	0.00372	0.00215	0.00253	0.00131	0.00165	**0.00129**
bottom-70%	0.00610	0.00239	0.00151	0.00178	**0.00075**	0.00103	0.00091
bottom-90%	0.00690	0.00124	0.00093	0.00111	**0.00030**	0.00104	0.00056

Table 13: Bias of the attribution map at the pixel level on VOC2012-VGG16

Method	Grad_CAM	|Grad|	GI	GB	DeepSHAP	LIME	LRP
top-10%	0.02984	0.00764	0.00656	0.00563	0.00768	0.00864	**0.00461**
top-30%	0.01876	0.00405	0.00292	0.00253	0.00310	0.00554	**0.00159**
top-50%	0.01365	0.00267	0.00176	0.00154	0.00187	0.00387	**0.00092**
top-70%	0.00947	0.00162	0.00115	0.00098	0.00132	0.00272	**0.00065**
top-90%	0.00650	0.00061	0.00051	**0.00038**	0.00089	0.00172	0.00044
bottom-10%	0.00767	0.00869	0.00768	0.00865	0.00396	0.00580	**0.00288**
bottom-30%	0.00708	0.00483	0.00372	0.00406	0.00173	0.00344	**0.00117**
bottom-50%	0.00654	0.00330	0.00238	0.00261	0.00106	0.00223	**0.00072**
bottom-70%	0.00540	0.00219	0.00170	0.00185	0.00075	0.00153	**0.00054**
bottom-90%	0.00509	0.00120	0.00107	0.00122	0.00041	0.00114	**0.00040**

Table 14: Bias of the attribution map at the pixel level on VOC2012-VGG19

Method	Grad_CAM	|Grad|	GI	GB	DeepSHAP	LIME	LRP
top-10%	0.02564	0.00761	0.00672	0.00580	0.00802	0.00851	**0.00468**
top-30%	0.01991	0.00403	0.00301	0.00261	0.00337	0.00565	**0.00157**
top-50%	0.01517	0.00263	0.00181	0.00159	0.00205	0.00402	**0.00091**
top-70%	0.01139	0.00161	0.00118	0.00102	0.00143	0.00282	**0.00064**
top-90%	0.00799	0.00062	0.00053	**0.00043**	0.00096	0.00183	0.00045
bottom-10%	0.00932	0.00867	0.00782	0.00871	0.00442	0.00587	**0.00236**
bottom-30%	0.00764	0.00480	0.00378	0.00406	0.00193	0.00352	**0.00095**
bottom-50%	0.00683	0.00326	0.00243	0.00260	0.00120	0.00231	**0.00059**
bottom-70%	0.00630	0.00217	0.00173	0.00184	0.00084	0.00140	**0.00046**
bottom-90%	0.00649	0.00119	0.00109	0.00120	0.00043	0.00107	**0.00036**

E   MORE RESULTS OF THE QUANTIFICATION OF UNEXPLAINABLE FEATURE COMPONENTS

The following table provides the result of the quantification of unexplainable feature components with $\tau = 0.1$.

Table 15: Quantification of unexplainable feature components with $\tau = 0.1$.

Method	Grad	GI	GB	DeepSHAP	LIME	LRP	Pert
CIFAR10-LeNet	0.96821	1.10399	0.91546	1.10371	**0.67032**	1.08469	0.70177
CIFAR10-ResNet20	1.22212	1.28065	1.14596	1.26002	**1.05286**	-	1.13032
CIFAR10-ResNet32	1.22803	1.29324	1.16028	1.27681	**1.04412**	-	1.14261
CIFAR10-ResNet44	1.22382	1.26434	1.10411	1.24961	**1.02039**	-	1.10772
CIFAR10-ResNet56	1.22487	1.24123	1.11306	1.24146	**1.00916**	-	1.10122
VOC2012-AlexNet	1.02425	1.09375	1.04981	1.0809	**1.01942**	1.11513	1.04048
VOC2012-VGG16	1.18959	1.22715	1.22724	1.32364	**1.12339**	1.32674	1.12878
VOC2012-VGG19	**1.08084**	1.1226	1.10411	1.17121	1.08387	1.23784	1.13043
VOC2012-ResNet50	1.23345	1.24123	**1.2156**	1.23441	1.22411	-	1.25732
VOC2012-ResNet101	1.08592	1.09363	**1.07853**	1.07856	1.11289	-	1.23279

F   ATTRIBUTION MAPS OF MASKED IMAGES

Figure 6: Examples of attribution maps after spatial masking.

G   DETAILED RESULTS OF THE MUTUAL VERIFICATION

Table 16: Mutual verification on VOC2012-VGG19

Method	Grad	GI	GB	DeepSHAP	LIME	LRP
Grad	0.0000	1.6661	1.4054	1.4177	1.4142	1.4375
GI	1.6661	0.0000	1.4159	1.4008	1.4140	1.3437
GB	1.4054	1.4159	0.0000	1.5834	1.4244	1.5242
DeepSHAP	1.4177	1.4009	1.5835	0.0000	1.3691	**1.1106**
LIME	1.4142	1.4141	1.4245	1.3691	0.0000	1.3874
LRP	1.4375	1.3437	1.5243	**1.1106**	1.3874	0.0000

Table 17: Mutual verification on VOC2012-VGG16

Method	Grad	GI	GB	DeepSHAP	LIME	LRP
Grad	0.0000	1.6647	1.3992	1.4302	1.4142	1.4621
GI	1.6647	0.0000	1.4191	1.3711	1.4139	1.2649
GB	1.3992	1.4191	0.0000	1.5839	1.4260	1.5320
DeepSHAP	1.4302	1.3712	1.5840	0.0000	1.3824	**1.0636**
LIME	1.4142	1.4140	1.4261	1.3825	0.0000	1.3960
LRP	1.4621	1.2649	1.5321	**1.0636**	1.3960	0.0000

Table 18: Mutual verification on VOC2012-AlexNet

Method	Grad	GI	GB	DeepSHAP	LIME	LRP
Grad	0.0000	1.5540	1.3477	1.4348	1.4148	1.4851
GI	1.5541	0.0000	1.4344	1.3224	1.4113	**0.8341**
GB	1.3477	1.4344	0.0000	1.4477	1.4146	1.4573
DeepSHAP	1.4349	1.3225	1.4478	0.0000	1.3221	1.2251
LIME	1.4149	1.4115	1.4147	1.3222	0.0000	1.3916
LRP	1.4851	**0.8341**	1.4573	1.2250	1.3915	0.0000

Table 19: Mutual verification on VOC2012-ResNet50

Method	Grad	GI	GB	DeepSHAP	LIME
Grad	0.0000	1.6285	1.4143	1.6242	1.4143
GI	1.6285	0.0000	1.4137	**0.6537**	1.4139
GB	1.4143	1.4136	0.0000	1.4137	1.4238
DeepSHAP	1.6242	**0.6537**	1.4137	0.0000	1.4139
LIME	1.4144	1.4141	1.4240	1.4140	0.0000

Table 20: Mutual verification on VOC2012-ResNet101

Method	Grad	GI	GB	DeepSHAP	LIME
Grad	0.0000	1.6877	1.4136	1.6428	1.4145
GI	1.6877	0.0000	1.4140	**0.6778**	1.4139
GB	1.4136	1.4140	0.0000	1.4140	1.4275
DeepSHAP	1.6428	**0.6778**	1.4140	0.0000	1.4138
LIME	1.4146	1.4140	1.4277	1.4139	0.0000

Table 21: Mutual verification on CIFAR10-ResNet56

Method	Grad	GI	GB	DeepSHAP	LIME
Grad	0.0000	1.4183	1.4107	1.4135	1.4142
GI	1.4183	0.0000	1.4140	1.4104	1.4140
GB	1.4107	1.4140	0.0000	1.4128	1.3879
DeepSHAP	1.4135	1.4104	1.4128	0.0000	1.4097
LIME	1.4142	1.4140	1.3879	1.4098	0.0000

Table 22: Mutual verification on CIFAR10-ResNet44

Method	Grad	GI	GB	DeepSHAP	LIME
Grad	0.0000	1.3999	1.4128	1.4147	1.4141
GI	1.3999	0.0000	1.4125	1.4114	1.4143
GB	1.4128	1.4125	0.0000	1.4152	1.4175
DeepSHAP	1.4147	1.4114	1.4152	0.0000	1.4097
LIME	1.4142	1.4144	1.4152	1.4175	0.0000

Table 23: Mutual verification on CIFAR10-ResNet32

Method	Grad	GI	GB	DeepSHAP	LIME
Grad	0.0000	1.4259	1.4129	1.4117	1.4143
GI	1.4259	0.0000	1.4164	1.4113	1.4145
GB	1.4129	1.4164	0.0000	1.4144	1.4111
DeepSHAP	1.4117	1.4113	1.4144	0.0000	1.4117
LIME	1.4144	1.4145	1.4112	1.4117	0.0000

Table 24: Mutual verification on CIFAR10-ResNet20

Method	Grad	GI	GB	DeepSHAP	LIME
Grad	0.0000	1.3895	1.4010	1.4134	1.4143
GI	1.3895	0.0000	1.4140	1.4133	1.4145
GB	1.4010	1.4140	0.0000	1.4164	1.4382
DeepSHAP	1.4134	1.4133	1.4164	0.0000	1.4118
LIME	1.4144	1.4145	1.4382	1.4118	0.0000

Table 25: Mutual verification on CIFAR10-LeNet

Method	Grad	GI	GB	DeepSHAP	LIME	LRP
Grad	0.0000	1.5079	1.1955	1.4352	1.4130	1.4904
GI	1.5079	0.0000	1.4714	1.3025	1.4003	**0.7179**
GB	1.1955	1.4714	0.0000	1.4329	1.4249	1.4881
DeepSHAP	1.4352	1.3025	1.4329	0.0000	1.3958	1.3063
LIME	1.4131	1.4004	1.4249	1.3959	0.0000	1.3805
LRP	1.4904	**0.7179**	1.4881	1.3063	1.3804	0.0000